Resolution analysis of wide-azimuth angle decomposition for wave-equation migration

Gabriela Melo, Earth Resources Laboratory - Massachusetts Institute of Technology,*
Paul Sava, Center for Wave Phenomena - Colorado School of Mines

SUMMARY

Angle-dependent reflectivity constructed from an extended imaging condition, applied to the extrapolated source and receiver wavefields, can be employed to velocity/anisotropy estimation and amplitude versus angle (AVA) analysis. This imaging condition allows one to construct images as a function not only of three-dimensional position but also space lags of the source/receiver wavefield cross-correlation. The information in the space-lag domain can be mapped into the angle domain which is defined by the reflection and azimuthal angles at every image point. The relationship between sampling parameters in the angle and space-lag domain, together with the equations used to perform the mapping, show that the sample interval in the space-lag domain controls the range of angles that can be accurately recovered from the image. From the amplitude spectrum of the lag-domain common-image gathers, we can calculate the maximum angle that limits this range. The range of space-lags also influences the sampling interval in the angle domain. This analysis is important for the case where the angle-domain common-image gathers are employed for amplitude versus angle analysis. In this case, the amplitudes corresponding to the angles outside of this range would not be reliable, regardless of how accurate wavefield reconstruction is.

INTRODUCTION

In complex media, where velocity varies with position and may depend on direction of propagation, it is desirable to illuminate each location along the reflector from many directions in order to study how reflectivity changes with direction at the image point. Varying the surface azimuth as well as the surface source/receiver offset helps to illuminate different parts of the target at different angles. Some applications of wide-azimuth reflectivity are velocity analysis, amplitude versus angle analysis, and anisotropy estimation.

Salt bodies cause irregular illumination of targets located beneath them. This not only makes it difficult to properly image the shadow zones, but also creates spurious events in the images. Recently published work shows that it is possible to significantly improve image quality by acquiring and processing wide-azimuth data (Regone, 2006). The wide-azimuth data help to improve resolution in the velocity models (Michell et al., 2006; LaDart et al., 2006; Shoshitaishvili et al., 2006), identify directional fractures and attenuate coherent noise (Shirui et al., 2006), and consequently improve the image.

In general, a seismic reflection can be characterized by two parameters: reflection angle and azimuthal angle at the image point (assuming the reflector dips are known). These angles are defined locally at the image point and, in general, are not simply related to the surface parameters. The reflection plane is the plane containing the incident ray from the source to the reflection point, the normal to the reflector at this point, and the reflected ray from the reflection point to the receiver, all measured at the image point. This plane is defined in the vicinity of the image point. The angle between the incident/reflected ray and the normal is the reflection angle. The angle that characterizes the 3D orientation of the reflection plane in relation to a chosen direction, is the azimuthal angle.

Reflectivity information can be obtained by applying an imaging condition to the reconstructed source and receiver wavefields. One possible choice of imaging condition is a cross-correlation type imaging condition (Claerbout, 1971) that creates an image function of position in space. One possible way to construct angle-dependent reflectivity, i.e., reflectivity as a function of reflection and azimuthal angles, is through an extended imaging condition that preserves the orthogonal space lags from the source/receiver wavefield cross-correlation (Sava and Fomel, 2005) creating an image function of position in space and space lags. One can create space-lag-domain common-image gathers (lag gathers) from images obtained by extended imaging conditions, and then map the information from the lag domain to the angle domain, creating the so-called angle-domain common-image gathers (ADCIG or angle gathers). Events in angle gathers uniquely represent energy scattered from specific locations in the subsurface and are uniquely associated with pairs of incident and reflected rays that, in turn, uniquely define the reflector (Prucha et al., 1999; Stolk and Symes, 2002).

The goal of this work is to understand the relationship between the sampling parameters in both space-lag and angle domain and to establish the implications in the angle domain due to choices of sampling parameters in the space-lag domain. We obtain a reciprocal resolution/range relationship between lag and angle domain from the equations used to perform the lag to angle-domain mapping, together with the sampling parameters in both domains. First, this relationship shows that the resolution in the angle domain (which is associated with the sampling interval parameter in a sense that the smalles the sampling interval the better the resolution) is controlled by the range (which is associated with the number of samples times the sampling interval, i.e, the maximum value for the given variable) in the space-lag domain. Secondly, this relationship shows that the sampling interval in the space-lag domain controls the range of angles that can be accurately recovered from the image in the space-lag domain. Using these relationships, one can choose the parameters in both domains according to the desired resolution and range on angles for the ADCIGs.

As a synthetic example, we use the SEG/EAGE salt dome model to create data and images. In this example we show one common-image gather containing many reflections, where some of them are inside and some are outside the range of

accurately recoverd angles. The experimental results are consistent with our theoretical analysis.

THEORY

Migration of seismic data consists mainly of two parts: a wavefield reconstruction procedure that creates a source wavefield U_s and a receiver (scattered) wavefield U_r, at all space locations and all times (or frequencies) given a presumed velocity field; an imaging condition that extracts an image I (reflectivity information) from the reconstructed source and receiver wavefields, U_s and U_r. In order to construct angle-dependent reflectivity, one can employ an extended imaging condition that preserves space lags from the source/receiver wavefield cross-correlation. Here, we employ this extended imaging condition to obtain an image function of space and space lags,

$$I(\boldsymbol{x},\boldsymbol{\lambda}) = \sum_{\omega} U_r(\boldsymbol{x}+\boldsymbol{\lambda},\omega)U_s^*(\boldsymbol{x}-\boldsymbol{\lambda},\omega)\ , \qquad (1)$$

where $\boldsymbol{x} = (x, y, z)$ are the space coordinates, $\boldsymbol{\lambda} = (\lambda_x, \lambda_y, \lambda_z)$ are the cross-correlation space lags, ω is the temporal frequency, $U_s^*(\boldsymbol{x},\omega)$ is the complex conjugate of the source wavefield, $U_r(\boldsymbol{x},\omega)$ is the receiver wavefield, and $I(\boldsymbol{x},\boldsymbol{\lambda})$ is the extended image.

Next, we map the reflectivity information from the lag domain to the angle domain. In this work, we use the angle decomposition method based on the work of Sava and Fomel (2005). The relationship between the space lags $\boldsymbol{\lambda}$, and the reflection and azimuthal angles, θ and ϕ, in general, involves (k_x, k_y, k_z), the wavenumbers related to the space coordinates (x, y, z), and $(k_{\lambda_x}, k_{\lambda_y}, k_{\lambda_z})$, the wavenumbers related to the space lags $(\lambda_x, \lambda_y, \lambda_z)$. It is possible to avoid the vertical space lag λ_z by taking advantage of the fact that the wavenumber vectors $\boldsymbol{k_x}$ and $\boldsymbol{k_\lambda}$ are orthogonal (Sava and Fomel, 2005). This observation allows one to reduce the image $I(\boldsymbol{x},\boldsymbol{\lambda})$ from six to five dimensions by expressing λ_z as a function of the remaining 5 parameters.

Since the angle-domain common-image gathers are constructed from the space-lag-domain common-image gathers, it is important to understand the relationship between sampling in the angle and space-lag domains. We want to analyze the angle-domain resolution (sampling interval) and range (bounds), as functions of the sampling parameters in the space-lag domain. The resolution study involves understanding which parameters in the lag domain influences the resolution in the angle domain. The range analysis is meant to answer the question "What interval of angles can be accurately recovered for a given range and sampling in the lag-domain of migrated images obtained with an extended imaging condition?" Once the relationships between angle and space-lag-domain sampling parameters are established, it is possible to control resolution and range in the angle domain by choosing the corresponding parameters in the space-lag domain. This analysis has implications for establishing the maximum angle range that could potentially be used for AVA and MVA. Here, the analysis is limited to the case of horizontal reflectors.

In the case of a horizontal reflector, the wavenumbers k_x and k_y are zero and we have the following mapping equations

$$\theta = \arctan \frac{\sqrt{k_{\lambda_x}^2 + k_{\lambda_y}^2}}{k_z}\ , \qquad (2)$$

and

$$\phi = \arccos \frac{k_{\lambda_y}}{\sqrt{k_{\lambda_x}^2 + k_{\lambda_y}^2}}\ , \qquad (3)$$

where θ is the reflection angle and ϕ is the azimuthal angle. As mentioned earlier, these angles are related to a local geometry of source and receiver ray vectors at the image point.

For simplicity, let us assume that $k_{\lambda_y} = 0$ in equation 2. Theoretically, it is possible to map events in the angle-domain CIG for all reflection angles ranging from zero (corresponding to $k_{\lambda_x} = 0$) to 90° (corresponding to $k_z = 0$). From equation 2, for each fixed k_z, the maximum value of $\tan\theta$ mapped from the k_{λ_x} domain, corresponds to the maximum value of this wavenumber, $k_{\lambda_x^*} = 1/(2d_{\lambda_x})$. As k_z increases, the maximum value of $\tan\theta$ mapped from $k_{\lambda_x^*}$ decreases and it reaches a minimum for the maximum value of the depth wavenumber k_{z^*}. For a band-limited lag gather, k_{z^*} is the wavenumber that limits the band, i.e., k_{z^*} is the maximum k_z wavenumber. We define the angle corresponding to k_{z^*} and $k_{\lambda_x^*}$ by

$$\begin{aligned} \theta_F &= \arctan\left(\frac{k_{\lambda_x^*}}{k_{z^*}}\right) \\ &= \arctan\left(\frac{1}{2d_{\lambda_x}}\frac{1}{k_{z^*}}\right)\ , \end{aligned} \qquad (4)$$

where k_{z^*} and $k_{\lambda_x^*}$ are the maximum value for the depth and lag wavenumbers, respectively. In the (θ, k_z) domain, the angles for which we have information corresponding to all possible values of k_z are the angles $\theta < \theta_F$. The extreme case (or worst case scenario), that would have the smallest maximum value of $\tan\theta$ corresponding to $k_{\lambda_x^*}$, would be for a wide-band lag gather, with k_{z^*} corresponding to the Nyquist frequency, in which case $k_{z^*} = 1/(2d_z)$. Thus, not only k_{z^*}, but also the sampling interval in λ_x, controls θ_F. The angle θ_F defines the range of angles that can be accurately recovered from the lag-domain. For reflection angles greater than θ_F, there is energy defocusing and spreading away from the depth of the reflector in the CIGs due to edge effect in the (θ, k_z) domain. This phenomenon becomes more pronounced for increasing angles. Therefore, even if there is information in the lag gather corresponding to near grazing incidence (90° incidence angle) in the lag gather, when mapped to the angle domain, the energy corresponding to this event is defocused.

Equation 2 shows that, for each k_{λ_y} there is a different θ_F angle that can be mapped from the lag domain, given by $k_{\lambda_x^*}$ and k_{z^*}, that limits the range of angles for which there is information at all values of k_z. In 3D, we define θ_F as the smallest of these angles, which corresponds to $k_{\lambda_y} = 0$ in equation 2. This angle θ_F defines the range of reflection angles that can be accurately recovered from the lag domain, because this range of angles contains information for all depth wavenumbers k_z for all azimuths. The maximum θ for which there is information at all wavenumbers k_z changes with ϕ. Outside the range

defined by θ_F, due to the fact that this maximum θ changes with ϕ, there is an uneven information distribution along the ϕ dimension, with respect to k_z.

To study how the sampling interval for θ, d_θ, changes with k_{λ_x} and k_{λ_y}, we differentiate equation 2 first with respect to k_{λ_x}

$$d_\theta = \frac{k_z k_{\lambda_x}}{(k_z^2 + k_{\lambda_x}^2 + k_{\lambda_y}^2)\sqrt{k_{\lambda_x}^2 + k_{\lambda_y}^2}} \frac{1}{n_{\lambda_x} d_{\lambda_x}} , \quad (5)$$

and then with respect to k_{λ_y}

$$d_\theta = \frac{k_z k_{\lambda_y}}{(k_z^2 + k_{\lambda_x}^2 + k_{\lambda_y}^2)\sqrt{k_{\lambda_x}^2 + k_{\lambda_y}^2}} \frac{1}{n_{\lambda_y} d_{\lambda_y}} . \quad (6)$$

Similarly, to study how the sampling interval for ϕ, d_ϕ, changes with k_{λ_x} and k_{λ_y}, we differentiate equation 3 first with respect to k_{λ_x}

$$d_\phi = \frac{1}{\sqrt{1 + \frac{k_{\lambda_y}^2}{k_{\lambda_x}^2 + k_{\lambda_y}^2}}} \frac{-k_{\lambda_x} k_{\lambda_y}}{(k_{\lambda_x}^2 + k_{\lambda_y}^2)^{3/2}} \frac{1}{n_{\lambda_x} d_{\lambda_x}} \quad (7)$$

and then with respect to k_{λ_y}

$$d_\phi = \frac{1}{\sqrt{1 + \frac{k_{\lambda_y}^2}{k_{\lambda_x}^2 + k_{\lambda_y}^2}}} \frac{k_{\lambda_x}^2}{(k_{\lambda_x}^2 + k_{\lambda_y}^2)^{3/2}} \frac{1}{n_{\lambda_y} d_{\lambda_y}} \quad (8)$$

Equations 5, 6, 7, and 8 show that d_θ and d_ϕ are both inversely proportional to $n_{\lambda_x} d_{\lambda_x} = \lambda_x^*$ and $n_{\lambda_y} d_{\lambda_y} = \lambda_y^*$, where the parameters λ_x^* and λ_y^* are the ranges in space-lag domain, which control the resolution in the angle domain. Thus, we conclude that the larger the range in the space-lag domain, the better the resolution in the angle domain.

According to the analysis performed here, we conclude that when implementing the extended imaging condition one should use the smallest samplimg interval that is available for the space lags, which is the same sampling interval as for the corresponding space coordinates.

EXAMPLES

We present a synthetic example of angle decomposition analysis using the SEG/EAGE salt dome model to create the data and the images. Here, we use the Split Step Fourier downward-continuation method (Stoffa et al., 1990) to migrate the data. In this example, we show one CIG containing many reflections, where some of them are inside and some are outside the range of accurately recovered angles. In this CIG we can see the difference between the amplitudes corresponding to the reflection angles inside and outside of the range.

We use the SEG/EAGE salt dome model as velocity and reflectivity model to create synthetic data. Figure 1 shows the the location of 31 sources in relation to the CIG location. Figure 2 shows the velocity and reflectivity model. Figure 3 shows the migrated image. The point where the horizontal lines cross in Figure 2 and Figure 3 show the location of the CIG. We use

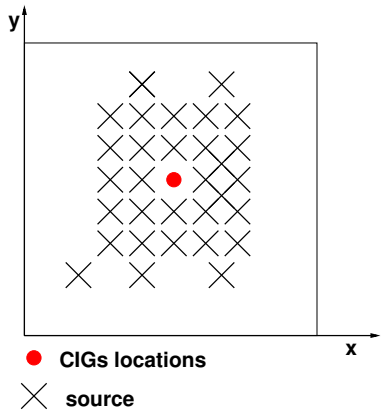

Figure 1: CIG locations. Each circle is a CIG location and the cross is the source location. There are 31 sources not uniformly spaced.

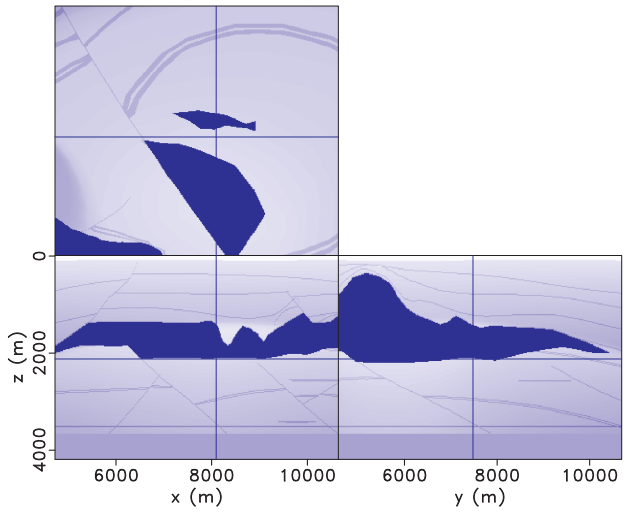

Figure 2: Velocity and reflectivity model for SEG/EAGE salt dome model.

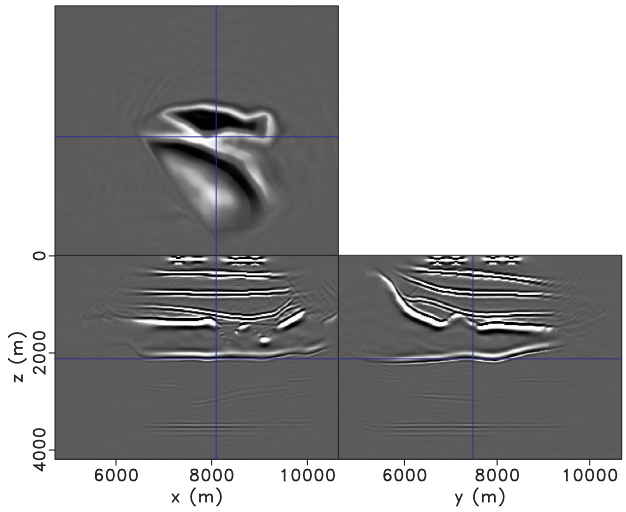

Figure 3: Migrated image for SEG/EAGE salt dome model.

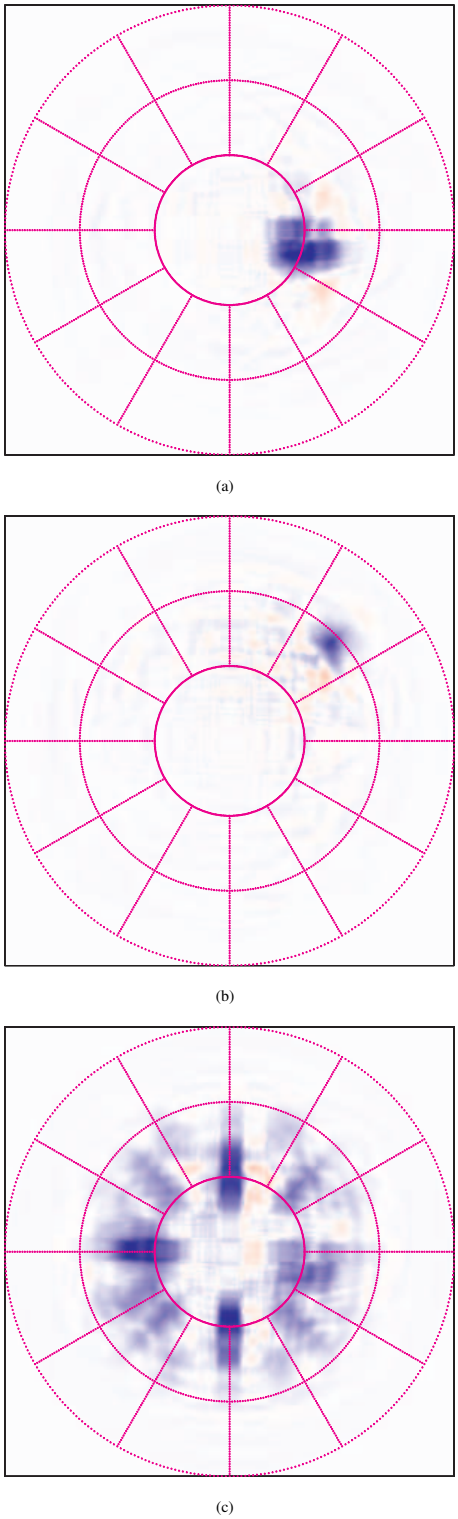

Figure 4: Polar representation of angle-domain common-image gathers for SEG/EAGE salt dome model. (a) and (b) are CIGs for two different individual shots for the same reflector location. (c) is the CIG for the same reflector location, but accounting for all the shots. Note in (c) that the amplitude for the reflection corresponding to figure (b) is weaker in (c) whereas the amplitude for the reflection in (a) is strong in (c).

31 shots distributed around the CIG location. The range size of the horizontal axis x and y for each shot is $x = y = 4000$ m. In this example we constructed the CIGs with 30 grid points on the lag axis, so $\lambda_x^* = \lambda_y^* = 300$ m.

Figure 4(a) shows the angle-domain CIG for one shot. The reflection angle in this case is approximately $\theta = 30^\circ$. Figure 4(b) shows the angle-domain CIG for another shot location. The reflection angle in this case is approximately $\theta = 55^\circ$. In both figures we clearly see the reflections. Figure 4(c) shows the angle-domain CIG for all the 31 shots used for imaging. We clearly see the reflection corresponding to 30° but we barely see the reflection corresponding to 55°. Performing the range and resolution analysis studied in this work, we conclude that for this example, the bound of the range of usable angles would be $\theta_F = 35^\circ$. Thus, when all the CIGs are plotted together as in Figure 4(c) the amplitude of the reflection corresponding to $\theta = 30^\circ$, which is inside the range, is higher than the one corresponding to $\theta = 55^\circ$, which is outside the range. This difference in amplitude happens because for the reflection corresponding to $\theta = 55^\circ$, which is outside the range, the energy is not as well focused at the depth of the image point as for the case $\theta = 30^\circ$ due to the effect explained above.

CONCLUSIONS

According to the analysis performed in this work, we conclude that when implementing the extended imaging condition one should use the smallest sample interval that is available for the space lags, which is the same sample interval as for the corresponding space coordinates. This is convenient since conventional implementations of the extended imaging condition keeps the space and space-lag sampling intervals the same.

We obtain reciprocal resolution/range relationships between lag and angle domains from the equations used to perform the lag to angle-domain mapping, together with the sampling parameters in both domains. The relationships show that the the angle-domain resolution is controlled by the range in the space-lag domain and that the angle-domain range is controlled by the resolution in the space-lag domain. In general, the angle that limits this range is proportional to the ratio between maximum depth wavenumber and maximum space-lag wavenumber. This angle limits the range of reflection angles for which energy focuses at the depth of the reflector in the angle gathers. In 3D, this angle range varies with the azimuthal angle. The largest wavenumbers of the lag gather limit the range of angles for which one can trust the amplitudes in the angle gather. This is particularly important if these angle gathers are being employed to perform amplitude versus angle analysis or migration velocity analysis.

ACKNOWLEDGMENTS

We acknowledge the financial support of the sponsors of the Center for Wave Phenomena at Colorado School of Mines and the Statoil Hrydro grant.